Validation of an adjoint method for compressible channel flow sensitivities

L. MORET-GABARRO, P. CATHALIFAUD, C. AIRIAU

Université de Toulouse ; CNRS, INPT, UPS ; IMFT (Institut de Mécanique des Fluides de Toulouse); Allée Camille Soula, F-31400 Toulouse, FRANCE

Résumé :

Les méthodes adjointes peuvent être utilisées en dynamique des fluides pour faire de l'analyse de sensibilité, pour trouver les perturbations optimales d'un écoulement, ou encore pour mener une étude de contrôle optimal. Nous nous sommes intéressés ici aux équations adjointes de Navier-Stokes compressible, instationnaire, 2D, pour des écoulements en présence de parois solides. Des conditions adéquates sont données aux parois, et le système direct-adjoint a été validé pour un écoulement de canal plan. Ce cas test académique consitue la première étape avant de passer à des cas d'écoulements plus complexes.

Abstract :

Adjoint methods are used in fluid dynamics to perform sensitivity analysis, to find optimal perturbations and to apply optimal control theory. In this study the adjoint of the 2D unsteady compressible Navier-Stokes equations are applied to wall bounded flows. Suitable wall boundary conditions for the adjoint equations are derived and the whole direct-adjoint system is validated for a plane channel flow. This academic test case is the first step to perform adjoint analysis of more complex flows.

Key-words : Aeroacoustics, Direct Numerical Simulation, Adjoint methods

1 Introduction

Recent rise in aviation transport and environmental concern has caused a growing interest for aeroacoustic investigations and flow control for noise and drag reduction, for instance in jet flows and wall-bounded configurations with an industrial application.
The study of closed-loop control by numerical methods is limited by the capacity of computers. In complex three-dimensional configurations its application is currently difficult due to the amount of data and computational time required. For this reason, closed-loop control on reduced order models and open-loop control strategies are being investigated.
Adjoint methods are used in fluid dynamics to perform receptivity and sensitivity analysis, to find optimal perturbations and open-loop optimal control. Most of the prior studies have focused on incompressible flows, but more recently the adjoint of the unsteady compressible Navier-Stokes equations have been used in free shear flows for sensitivity analysis [1, 2] and flow control [3], and the adjoint of a semi-discretized system has been used for control in bounded flows [4].
In this study an approach to test the accuracy and to validate simultaneously the direct and the adjoint equations is proposed, where the adjoint of the 2D unsteady compressible Navier-Stokes equations are applied to wall bounded flows. Appropriate wall boundary conditions for the adjoint equations are derived and the whole direct-adjoint system is validated for a plane channel flow. This academic test case is the first step to perform adjoint analysis of more complex flows of industrial interest, as cavities or airfoils.

2 Governing equations

2.1 Navier-Stokes equations

This study is done by Direct Numerical Simulation of the 2D unsteady compressible Navier-Stokes equations with conservative variables $q = [\rho, \rho u, \rho v, p]$, where ρ is the density, $\rho u = m_x$ and $\rho v = m_y$ are the x- and y-momentum and p is the pressure. The dimensional governing equations are:

$$\frac{\partial \rho}{\partial t} + \frac{\partial m_x}{\partial x} + \frac{\partial m_y}{\partial y} = 0$$

$$\frac{\partial m_x}{\partial t} + \frac{\partial(\rho u^2)}{\partial x} + \frac{\partial(\rho uv)}{\partial y} + \frac{\partial p}{\partial x} - \left(\frac{4}{3}\frac{\partial}{\partial x}(\mu\frac{\partial u}{\partial x}) + \frac{\partial}{\partial y}(\mu\frac{\partial v}{\partial x} + \mu\frac{\partial u}{\partial y}) - \frac{2}{3}\frac{\partial}{\partial x}(\mu\frac{\partial v}{\partial y})\right) = 0$$

$$\frac{\partial m_y}{\partial t} + \frac{\partial(\rho uv)}{\partial x} + \frac{\partial(\rho v^2)}{\partial y} + \frac{\partial p}{\partial y} - \left(\frac{4}{3}\frac{\partial}{\partial y}(\mu\frac{\partial v}{\partial y}) + \frac{\partial}{\partial x}(\mu\frac{\partial v}{\partial x} + \mu\frac{\partial u}{\partial y}) - \frac{2}{3}\frac{\partial}{\partial y}(\mu\frac{\partial u}{\partial x})\right) = 0$$

$$\frac{\partial p}{\partial t} + \frac{\partial(pu)}{\partial x} + \frac{\partial(pv)}{\partial y} + (\gamma-1)\,p\left(\frac{\partial u}{\partial x} + \frac{\partial v}{\partial y}\right) - (\gamma-1)\frac{c_p}{Pr}\left(\frac{\partial}{\partial x}(\mu\frac{\partial T}{\partial x}) + \frac{\partial}{\partial y}(\mu\frac{\partial T}{\partial y})\right) - \Phi_\nu = 0.$$

where μ is the dynamic viscosity which depends on the temperature T, γ is the ratio of specific heats, $Pr = 0.72$ is the Prandlt number considered constant, c_p is the specific heat at constant pressure and Φ_ν is the viscous dissipation term of the energy equation. The system can be writen as $\dot{q} + NS(q) = 0$.

2.2 Adjoint equations

Sensitivity analysis and optimal control are related to the energy of the mean flow variables, represented by the cost function:

$$\mathcal{J} = \frac{1}{2}\langle q, q\rangle \tag{1}$$

where the inner product $\langle ., . \rangle$ is defined over the whole space-time domain. From a variational approach, the linear equations for the small perturbations of the mean flow are used to derive the adjoint equations. In order to minimize the energy of the perturbations, the following Lagrangian function is used:

$$\mathcal{L} = \frac{1}{2}\langle q, q\rangle + \langle \xi, \dot{q} + NS(q)\rangle \tag{2}$$

where the Lagrangian multipliers ξ are the adjoint variables. The solutions of the minimization problem are:

$$\begin{aligned} \frac{\partial \mathcal{L}}{\partial \xi} &= \dot{q}' - Aq' \qquad \text{Direct equations} \\ \frac{\partial \mathcal{L}}{\partial q} &= q' - \dot{\xi} - A^*\xi \quad \text{Adjoint equations} \end{aligned} \tag{3}$$

where $q' = [\rho', (\rho u)', (\rho v)', p']$ are small perturbations of the flow and A is the Jacobian matrix of the Navier-Stokes equations $A = \partial NS/\partial q$. To derive the adjoint equations two simplifications have been made: viscosity μ is assumed to be constant and the viscous dissipation term of the energy equation Φ_ν has been neglected [1]. These simplifications are based on the assumption that spatial and temporal variations of viscosity and viscous dissipation in the heat equation do not have an important effect on sound propagation, since they take place only at small length scales [1]. The adjoint equations are linear, they are run backward in time and the adjoint state vector is $\xi = q^* = [p^*, (\rho u)^*, (\rho v)^*, \rho^*]$. Note that adjoint pressure is related to the continuity equation, while adjoint density is related to the energy equation. The adjoint equations are expressed as:

$$-\frac{\partial \rho^*}{\partial t} - u\frac{\partial \rho^*}{\partial x} - v\frac{\partial \rho^*}{\partial y} - \frac{\partial m_x^*}{\partial x} - \frac{\partial m_y^*}{\partial y} + (\gamma-1)\rho^*\left(\frac{\partial u}{\partial x} + \frac{\partial v}{\partial y}\right) - \frac{\gamma\mu}{Pr}\frac{1}{\rho}\left(\frac{\partial^2 \rho^*}{\partial x^2} + \frac{\partial^2 \rho^*}{\partial y^2}\right) = 0$$

$$-\frac{\partial m_x^*}{\partial t} - 2u\frac{\partial m_x^*}{\partial x} - v\left(\frac{\partial m_y^*}{\partial x} + \frac{\partial m_x^*}{\partial y}\right) - \frac{\partial p^*}{\partial x} - \gamma\frac{p}{\rho}\frac{\partial \rho^*}{\partial x} - (\gamma-1)\frac{\rho^*}{\rho}\frac{\partial p}{\partial x} - \frac{\mu}{\rho}\left(\frac{4}{3}\frac{\partial^2 m_x^*}{\partial x^2} + \frac{\partial^2 m_x^*}{\partial y^2} + \frac{1}{3}\frac{\partial^2 m_y^*}{\partial x \partial y}\right) = 0$$

$$-\frac{\partial m_y^*}{\partial t} - 2v\frac{\partial m_y^*}{\partial y} - u\left(\frac{\partial m_y^*}{\partial x} + \frac{\partial m_x^*}{\partial y}\right) - \frac{\partial p^*}{\partial y} - \gamma\frac{p}{\rho}\frac{\partial \rho^*}{\partial y} - (\gamma-1)\frac{\rho^*}{\rho}\frac{\partial p}{\partial y} - \frac{\mu}{\rho}\left(\frac{4}{3}\frac{\partial^2 m_y^*}{\partial y^2} + \frac{\partial^2 m_y^*}{\partial x^2} + \frac{1}{3}\frac{\partial^2 m_x^*}{\partial x \partial y}\right) = 0$$

$$\begin{aligned} -\frac{\partial p^*}{\partial t} + \gamma\frac{p}{\rho}\left(u\frac{\partial \rho^*}{\partial x} + v\frac{\partial \rho^*}{\partial y}\right) + u^2\frac{\partial m_x^*}{\partial x} + v^2\frac{\partial m_y^*}{\partial y} + uv\left(\frac{\partial m_x^*}{\partial y} + \frac{\partial m_y^*}{\partial x}\right) + (\gamma-1)\frac{\rho^*}{\rho}\left(u\frac{\partial p}{\partial x} + v\frac{\partial p}{\partial y}\right) \\ +\mu\frac{u}{\rho}\left(\frac{4}{3}\frac{\partial^2 m_x^*}{\partial x^2} + \frac{\partial^2 m_x^*}{\partial y^2} + \frac{1}{3}\frac{\partial^2 m_y^*}{\partial x \partial y}\right) + \mu\frac{v}{\rho}\left(\frac{4}{3}\frac{\partial^2 m_y^*}{\partial y^2} + \frac{\partial^2 m_y^*}{\partial x^2} + \frac{1}{3}\frac{\partial^2 m_x^*}{\partial x \partial y}\right) + \frac{\gamma\mu}{Pr}\frac{p}{\rho^2}\left(\frac{\partial^2 \rho^*}{\partial x^2} + \frac{\partial^2 \rho^*}{\partial y^2}\right) = 0 \end{aligned}$$

Both systems are discretized using a 6^{th} order compact scheme in space and 4^{th} order Runge-Kutta scheme in time. Characteristic conditions are used at the non-reflecting boundaries: the formulation proposed by Giles [5] is used for the direct system, and an equivalent formulation derived by Spagnoli[6] is implemented for the adjoint system.

2.3 Wall boundary conditions

The adjoint equations are derived from the minimization of the Lagrangian function defined by equation (2), which is solved by integration by parts. As a result, some boundary terms appear. In order to simplify the numerical implementation, the boundary terms can be cancelled by selecting the appropriate boundary conditions. For a solid boundary, imposing the non-slip condition $u = v = 0$, and the isothermal $\delta T = 0$ or the adiabatic $\partial T/\partial y = 0$ condition, it is found that the conditions over the adjoint variables in order to make the boundary terms equal to zero should be:

$$\begin{aligned} (\rho u)^* = (\rho v)^* = \rho^* = 0 \qquad & \text{isothermal} \\ (\rho u)^* = (\rho v)^* = \frac{\partial \rho^*}{\partial y} = 0 \qquad & \text{adiabatic} \end{aligned} \tag{4}$$

3 Sensitivities and validation

The DNS code used to obtain the direct results was previously validated by Guaus [7, Appendix A], so only the validation of the adjoint system is to be described and shown.
The adjoint equations of a direct problem satisfy the Green-Lagrange identity:

$$\langle q^*, f \rangle = \langle g, q' \rangle \tag{5}$$

where g and f are the forcing of the adjoint and direct systems respectively. If the direct system is used to force the adjoint, i.e. taking $g = q$, then equation (5) becomes:

$$\langle q^*, f \rangle = \langle q, q' \rangle = \delta \mathcal{J} \tag{6}$$

That is to say, q^* is the adjoint of q, which is the gradient of the cost function $\mathcal{J}$ respect to the forcing f. So forcing an adjoint equation gives the sensitivity of the corresponding direct variable, which is equivalent to the effect on the adjoint field caused by forcing the direct system. As a consequence, the adjoint formulation can be validated by forcing both systems with the same function and comparing the resulting fields.
For more details on the theory the reader is refered to [2].
As a first validation test, the x-momentum sensitivity field is selected, for which it is required to force the x-momentum equation:

$$\int_T \int_\Omega (\rho u)^* \, f_2 \, d\Omega dt = \int_T \int_\Omega g_2 \, (\rho u)' \, d\Omega dt \tag{7}$$

Since the main objective of developing this adjoint method is to perform noise control, the results for the sensitivity of pressure are of interest, for which adjoint density must be forced. On the left hand side, it is arbitrarily chosen to force the density equation:

$$\int_T \int_\Omega p^* f_1 \, d\Omega dt = \int_T \int_\Omega g_4 p' \, d\Omega dt \tag{8}$$

For the present investigation, a time-periodic Gaussian pulse of amplitude A is inserted in the center of a plane channel:

$$f = g = A \, \sin(\omega t) \, G(x, y) \tag{9}$$

$$G(x, y) = \exp \frac{\left[\left(x^2 + y^2 \right) \right]}{\sigma^2}$$

Since the flow is symmetric, if the same frequency and amplitude are selected for both systems, the resulting fields will be symmetric with respect to the vertical center line of the channel and respect to the time. Consequently, the temporal evolution of the spatial integration can be compared as:

$$\int_T \overline{(\rho u)^*} \sin(\omega t_i) \, dt_i \approx \int_T \overline{(\rho u)'} \sin(\omega t) \, dt \tag{10}$$

where

$$\overline{(\rho u)^*} = \int_\Omega (\rho u)^* \, G(x,y) d\Omega \qquad \overline{(\rho u)'} = \int_\Omega (\rho u)' \, G(x,y) d\Omega$$

where the time for the adjoint is $t_i = t_T - t$, with t_T the terminal time. An equivalent expression is used to compare the temporal evolution of the spatial integration of pressure when the forcing is applied to the density and adjoint density equations.

4 Results: channel flow

4.1 Direct and adjoint forcing

In order to validate the adjoint method a laminar plane channel flow is used. The computational domain is shown in figure 1, as well as the initial perturbation for both the direct and adjoint simulations. The grid is equidistant and contains 100x100 points.
Two simulations are required in order to obtain the fluctuation fields of the direct system. Firstly, the simulation is computed without any perturbation, in order to get the 'nominal' (reference) flow. Its initial condition is the analytical solution for a Poiseuille incompressible channel flow. Secondly, the simulation is calculated applying the periodic perturbation to the right-hand-side of the Navier-Stokes equations, giving the 'perturbed' field. Taking the difference of these two fields the fluctuations are obtained.
Since the adjoint equations are linear, only one simulation is necessary to obtain the adjoint results. In the adjoint simulations, all variables are initialized as zero except the one where the forcing is applied.

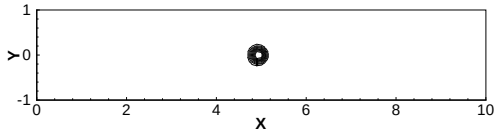

Figure 1: Computational domain and isocontours of pressure and adjoint pressure at initial time: $M = 0.4$.

Several test cases have been performed to study the sensitivity of x-momentum and pressure, according to equations (7) and (8), using both wall boundary conditions, at two different Mach numbers ($M = 0.1$ and $M = 0.4$). The Reynolds number based on the half-width of the channel is $Re_H = 14$ for $M = 0.1$ and $Re_H = 58$ for $M = 0.4$, unless stated otherwise.
The sensitivity of pressure at $M = 0.4$ and using adiabatic wall boundary conditions is used to illustrate the symmetry of the flow. For this test case, the parameters of the forcing from eq.(9) are $A = 0.01\rho_\infty$, $\omega = 2\pi/50\Delta t$ and $\sigma = 10\Delta y$.
Figure 2 shows the two-dimensional fields for the direct and adjoint computations after periods 1 and 5. In the direct computations (on the left), the flow is moving from left to right, and so the pressure fluctuations are propagated to the right. On the other hand, in the adjoint simulations (on the right) the time is inverted, and hence the pressure perturbation is convected to the left. The results at these two different times show very good qualitative agreement between direct and adjoint simulations.

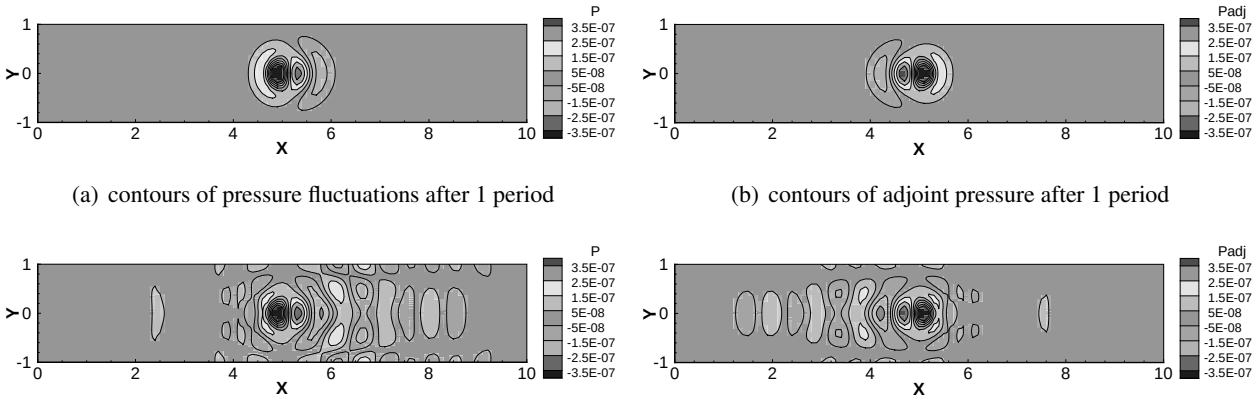

(a) contours of pressure fluctuations after 1 period

(b) contours of adjoint pressure after 1 period

(c) contours of pressure fluctuations after 5 periods

(d) contours of adjoint pressure after 5 periods

Figure 2: Comparison of the isocontours of pressure: adiabatic wall, $M = 0.4$.

4.2 Sensitivity of *x*-momentum

Several test cases have been computed applying forcing of *x*-momentum, using adiabatic and isothermal wall boundary conditions and Mach numbers 0.1 and 0.4. All test cases have the same forcing parameters in eq.(9): $A = 0.01U_\infty$, $\omega = 2\pi/100\Delta t$ and $\sigma = 10\Delta y$, and have been run during 10 periods of the perturbation, in which the pulse reaches the solid and the non-reflecting boundaries.

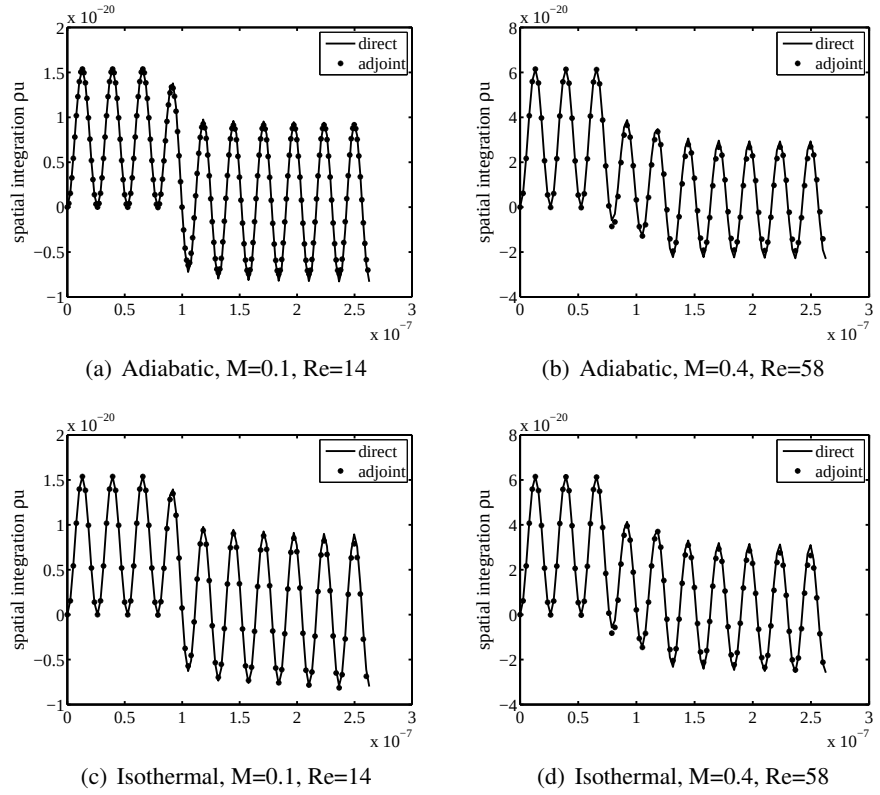

(a) Adiabatic, M=0.1, Re=14

(b) Adiabatic, M=0.4, Re=58

(c) Isothermal, M=0.1, Re=14

(d) Isothermal, M=0.4, Re=58

Figure 3: Comparison of the temporal evolution of the spatial integration: *x*-momentum.

Since the flow is symmetric, and the same frequency and amplitude are selected for both systems, the resulting fields are symmetric with respect to the vertical center line of the channel and respect to the time. Consequently, the temporal evolution of the spatial integration of *x*-momentum defined in eq.(10) can be compared as shown in figure 3.
In all cases it is observed that there is a sudden change of the mean amplitude value after approximately three periods. This instant in time corresponds to the moment when the pulse reaches for the first time the outflow non-reflecting boundary. It is shown that in all cases the agreement between direct and adjoint is good. There is also very good agreement between the simulations computed using adiabatic wall boundary conditions (subfigures 3(a) and 3(b)) and the corresponding results with an isothermal wall (subfigures 3(c) and 3(d)).

4.3 Sensitivity of pressure

Three test cases have been performed by forcing density, using adiabatic wall boundary conditions and Mach numbers 0.1 and 0.4. All test cases have the same forcing parameters in eq.(9): $A = 0.01\rho_\infty$, $\omega = 2\pi/50\Delta t$ and $\sigma = 10\Delta y$, and have been run during 10 periods of the perturbation, in which the pulse reaches the solid and the non-reflecting boundaries.
The temporal evolution of the spatial integration of pressure is given by eq.(10) replacing *x*-momentum by pressure. Figure 4 shows the results for the three cases.
The results from 4(a) and 4(b) have the same Mach number but different Reynolds number, so viscous effects can be compared. Both figures show a similar tendency of the temporal evolution of the integration of pressure. The direct results oscillate with small amplitude during the first 6 periods, and the amplitude becomes bigger after that. The change corresponds to the moment where the pulse reaches the non-reflecting boundaries. The adjoint do not present significant oscillations during the first periods, and after reaching the inflow and outflow start oscillating with bigger amplitude than the direct results. This amplitude of oscillation increases with Reynolds number.
The results from 4(b) and 4(c) have been computed using the same Reynolds number but different Mach number, in order to study the compressibility effects. The results for a Mach number 0.4 present an evolution similar to a Mach 0.1 during the first periods. After the perturbation reaches the non-reflecting boundaries, the

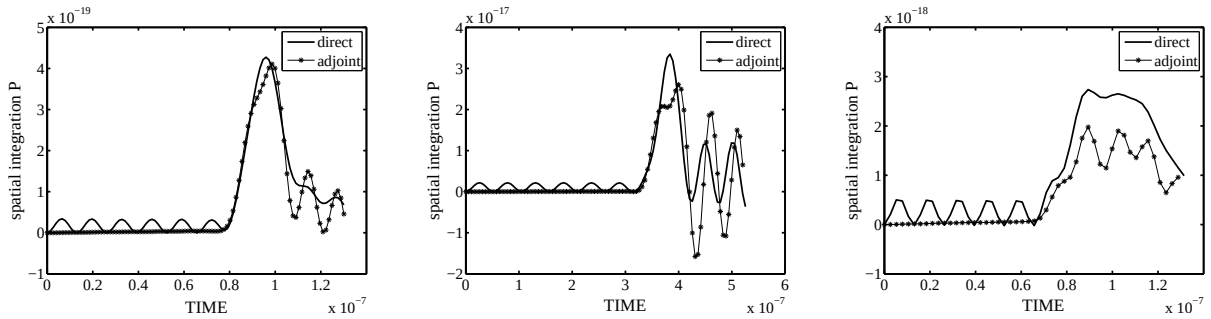

(a) Adiabatic, M=0.1, Re=14 (b) Adiabatic, M=0.1, Re=58 (c) Adiabatic, M=0.4, Re=58

Figure 4: Comparison of the temporal evolution of the spatial integration: pressure.

value of the integration increases and decreases without significant oscillations. In this case, the adjoint results follow the tendency of the direct but underestimate the values.
The differences observed between direct and adjoint simulations are thought to be related to the two simplifications assumed to derive the adjoint equations (viscosity is taken as constant and the viscous dissipation term of the energy equation is neglected). Another possible reason for the deviations could be the wall boundary condition, since some differences can be seen in figure 2 near the walls.
In conclusion, the comparison between direct and adjoint simulations show that the sensitivities of pressure fluctuations, obtained by forcing the density equation, are less accurate than the fluctuations of x-momentum.

5 Conclusions and future work

Adjoint analysis of a wall bounded flow has been performed, giving good agreement of the sensitivity of x-momentum. The results of the sensitivity of pressure are less accurate, suggesting that the numerical implementation could be improved. The next step of the investigation will be a sensitivity analysis to find which perturbation creates higher noise levels at the core flow, i.e. at a position far from the wall. This academic test case is the first step to perform adjoint analysis of more complex flows of industrial interest, as cavities or airfoils.

Acknowledgements

This research project has been supported by a Marie Curie EST Fellowship of the European Community's Sixth Framework Programme under contract number MEST CT 2005 020301. Special thanks to Anaïs Guaus for useful discussions.

References

[1] Cerviño L., Bewley T., Freund J., and Lele S. Perturbation and adjoint analyses of flow-acoustic interactions in an unsteady 2D jet. In Proceedings of the summer program 2002, pages 27–40. Center for Turbulence Research, 2002.

[2] Spagnoli B. and Airiau C. Adjoint analysis for noise control in a two-dimensional compressible mixing layer. Comp. Fluids, 37, 475–486, 2008.

[3] Wei M. and Freund J. A noise-controlled free shear flow. J. Fluid Mechanics, 546, 123–152, 2006.

[4] Collis S., Ghayour K., Heikenschloss M., Ulbrich M., and Ulbrich S. Optimal control of unsteady compressible viscous flows. Int. J. for Numerical Methods in Fluids, 40, 1401–1429, 2002.

[5] Giles M. Nonreflecting boundary conditions for euler equation calculations. AIAA Journal, 28(12), 2050–2058, 1990.

[6] Spagnoli B. Etude numérique de sensibilité et contrôle optimal du bruit aéroacoustique généré par une couche de mélange compressible bidimensionelle. PhD thesis, Université Paul Sabatier, Toulouse, France, November 2006.

[7] Guaus A. Analyse linéaire des instabilités dans les écoulements incompressibles à parois courbes compliantes. PhD thesis, Université Paul Sabatier, Toulouse, France, 2008.